Geophysical Research Letters

RESEARCH LETTER
10.1029/2024GL112196

Energetic Constraints on Baroclinic Eddy Heat Transport With a Beta Effect in the Laboratory

Cheng Qian[1], **Peter L. Read**[1], **and David P. Marshall**[1]

[1]Department of Physics, University of Oxford, Oxford, UK

Key Points:

- Energetic constraints on baroclinic eddy heat transport are tested in rotating annulus experiments
- Eddy buoyancy transport is bounded by total eddy energy with an approximate linearity when there is a beta effect
- The results without the beta effect are more complicated and may suggest extra variable dependencies

Supporting Information:

Supporting Information may be found in the online version of this article.

Correspondence to:

C. Qian,
cheng.qian@physics.ox.ac.uk

Citation:

Qian, C., Read, P. L., & Marshall, D. P. (2025). Energetic constraints on baroclinic eddy heat transport with a beta effect in the laboratory. *Geophysical Research Letters*, *52*, e2024GL112196. https://doi.org/10.1029/2024GL112196

Received 28 AUG 2024
Accepted 1 JAN 2025

Abstract Hypotheses involving energetic constraints and the down-gradient diffusion of heat in eddy parameterization theories are tested by estimating baroclinic eddy transports in rotating annulus laboratory experiments. Particle Imaging Velocimetry measurements are supplemented by numerical simulations to estimate variables not measured directly. The results with a topographic beta effect broadly support Fick's first law, and are consistent with the GEOMETRIC framework in which eddy buoyancy flux is constrained by total eddy energy. With the topographic beta effect, a relatively simple relation is observed between the eddy buoyancy flux and the total eddy energy, with the ratio quantifying the eddy transport efficiency. This efficiency decreases in more complex flow regimes with larger rotation rates, associated with the changing energy partition between eddy available potential energy and eddy kinetic energy. In the absence of a topographic beta effect, more complicated dependencies are found, suggesting roles for other variables.

Plain Language Summary Baroclinic instability is the geophysical process responsible for generating mid-latitude weather systems in the atmosphere, mesoscale eddies in the ocean, and also eddies in the atmospheres of Mars and other planets. It is challenging, however, for computational global climate models to resolve ocean eddies accurately and routinely, because they occur on relatively small spatial scales. The contribution of ocean eddies to the transport of heat and other tracers is typically represented in such models by simple "parameterizations," based on theories of the instability generating these eddies. These parameterizations are difficult to validate using observations in the ocean. In this study, eddy heat transports are measured in the laboratory to test key hypotheses and assumptions underpinning eddy parameterizations implemented in global coupled atmosphere-ocean climate models used to make climate projections and evaluate climate risks. This study provides the first direct experimental evidence that eddy heat transports are constrained by eddy energies.

1. Introduction

Baroclinic instability describes the transfer of energy from large-scale atmospheric and oceanic flows to transient eddies, and is the geophysical process responsible for generating mid-latitude weather systems and mesoscale ocean eddies (Lorenz, 1955, 1967; J. Marshall & Plumb, 2007; Vallis, 2017), as well as eddies in the atmospheres of Mars (Leovy, 1969) and other planets (Hide, 1977). However, it remains computationally unfeasible to fully and routinely resolve ocean mesoscale eddies in ocean-only and global coupled atmospheric/ocean climate models that run to mature thermodynamic and dynamical equilibrium over thousands of years.

The eddy parameterization problem is essentially to represent quantitatively unresolved eddy fluxes of buoyancy and other quantities in terms of large-scale resolved variables. This study aims to test the assumptions underlying classical and modern eddy parameterization schemes, including the downgradient flux-gradient relation (consistent with Fick's first law) as well as the energetic bounds inferred from GEOMETRIC theory. In this study, we then quantify the efficiencies of baroclinic eddy heat transport.

Fick's first law hypothesizes a linear dependence of diffusive flux of a tracer on its mean gradient (Green, 1970; Stone, 1972) and is a key ingredient underpinning most eddy parameterization theories (Green, 1970; Pfeffer & Barcilon, 1978), including the GM eddy parameterization (Gent & McWilliams, 1990; Gent et al., 1995) employed in many ocean climate models. Visbeck et al. (1997) extended the representation of the eddy transfer coefficient in the GM parameterization using the Eady growth rate of linear baroclinic instability (Eady, 1949). Further advances in representing the eddy transfer coefficient were proposed by Eden and Greatbatch (2008) and D. P. Marshall and Adcroft (2010) to constrain the magnitude of this coefficient by the eddy kinetic energy. Most recently, among other development frameworks for eddy parameterization toward this direction, GEOMETRIC

theory (D. P. Marshall et al., 2012) employs the energetic constraint on the buoyancy fluxes, which can be used, in turn, to constrain the GM eddy transfer coefficient in terms of the total (kinetic plus potential) eddy energy. Numerical calculations have demonstrated that the GEOMETRIC scheme has better capability to capture both linear and nonlinear regimes of baroclinic instability (Bachman et al., 2017). Moreover, the GEOMETRIC is able to reproduce the phenomenon of eddy saturation, in which the volume transport Antarctic Circumpolar Current exhibits limited sensitivity to surface wind stress (D. P. Marshall et al., 2017; Mak et al., 2017, 2018, 2022).

Specifically, the energetic constraint in the GEOMETRIC theory (D. P. Marshall et al., 2012) bounds the eddy buoyancy flux by the total eddy energy E as:

$$\left|\overline{b'v'}\right| = \alpha N_0 E, \tag{1}$$

where $\alpha \leq 1$ is a non-dimensional eddy transfer coefficient which quantifies the efficiency of eddy transport, and N_0 is the buoyancy frequency. The eddy transport efficiency can be decomposed into the product of three components:

$$\alpha = \gamma_b \sin(2\lambda) \sin\left(\phi_b\right). \tag{2}$$

here the anisotropy parameter is $\gamma_b = \sqrt{\left(R^2 + S^2\right)/(KP)}N_0/\left(2f_0\right)$, where $R = \overline{u'b'}f_0/N_0^2$ and $S = \overline{v'b'}f_0/N_0^2$ are proportional to components of the eddy buoyancy flux. The K and P are respectively the eddy kinetic energy $\left(\overline{\mathbf{u}'^2}/2\right)$ and the eddy available potential energy $\left(\overline{b'^2}/\left(2N_0^2\right)\right)$, and the total eddy energy is $E = K + P$. The energy partition term is represented by $\sin(2\lambda) = 2\sqrt{KP/E^2}$ and the ϕ_b is the eddy tilt angle such that $\sin\left(\phi_b\right) = S/\sqrt{R^2 + S^2}$. These definitions of eddy tilt angle and anisotropy are not limited to isolated eddies but are also applicable to jet-dominated turbulent flow regions. Here α is bounded by 1 due to the triangle inequalities (D. P. Marshall et al., 2012):

$$\frac{N_0^2}{2f_0^2}\left(R^2 + S^2\right) \leq KP \leq \frac{E^2}{2}. \tag{3}$$

The eddy transports of heat and biochemical tracers are difficult to measure directly in the ocean. However, eddy heat transport can be determined, in principle, in controlled laboratory experiments, capable of achieving at least some level of dynamical similarity with atmospheric and oceanic flows (Read et al., 2014). Specifically, baroclinic eddy heat transport can be measured in a differentially heated rotating annulus (Hide & Mason, 1975; Hignett et al., 1985) to test the hypotheses and assumptions of eddy parameterization theories (Pérez et al., 2010; Read, 2003). Previous numerical studies have validated the theory underpinning the role of energetic constraints on eddy transport (Bachman et al., 2017; Mak et al., 2018). This study combines laboratory measurements with numerical simulations to investigate eddy heat transports in the presence and absence of a topographic beta effect and the extent to which Fick's law holds (Fultz & Kaylor, 1959; Hignett et al., 1985; Pérez et al., 2010; Vincze et al., 2014), and to test the GEOMETRIC relation (Equation 1) for the first time in the laboratory.

2. Methodology

Conditions to observe baroclinic eddies can be achieved in the laboratory with a differentially heated rotating annulus (Hide, 1953). The temperature difference across the annulus and the rotation rate can be varied to enable a systematic investigation to test the hypotheses of eddy parametrization theories accross a wide range of parameter regimes (Hide & Mason, 1975; Hignett et al., 1985; Mason, 1975), as detailed in Supporting Information S1 (Table S1). The impact of a beta effect is investigated by introducing a conically sloping upper topographic boundary; topographic beta effect is defined as $\beta_T = \left(2\Omega/\overline{H}\right)dH/dr$ following previous studies, for example, see the work of Fultz and Kaylor (1959), Mason (1975), Hignett et al. (1985), Bastin and Read (1997), Wordsworth et al. (2008), Isachsen (2011), von Larcher et al. (2013), and Vincze et al. (2014). Measurement results with the beta effect from the sloping topography are compared with those obtained in experiments with flat boundaries, henceforth referred to as the f-plane (Pérez et al., 2010; Read, 2003).

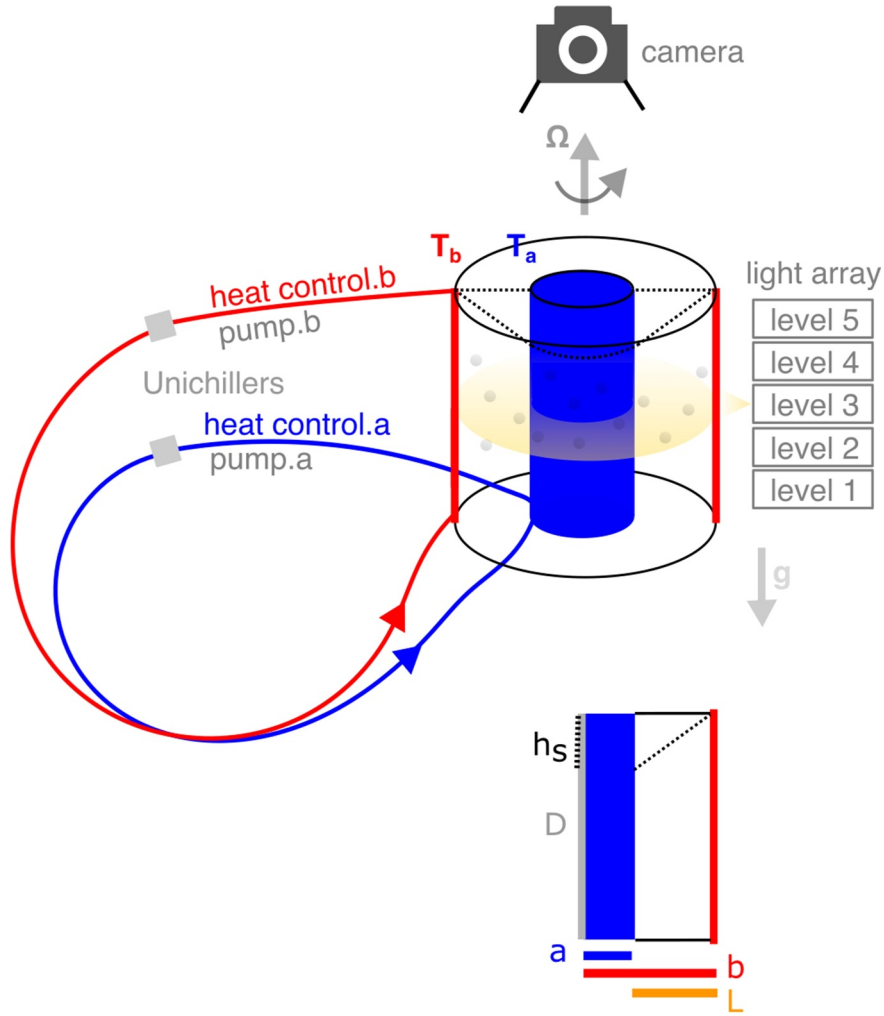

Figure 1. Measurement method. A schematic diagram shows the measurement of multi-level Particle Image Velocimetry (PIV). In the PIV experiment, a camera captured images of the reflective particles as the light array switched to discrete height levels (Wordsworth et al., 2008). The meridional plane of the annulus domain is illustrated in the bottom panel for the geometry of the annulus with the radial width (L = b − a) and height (D), as well as the geometry of the sloping topography with height (h_s).

In order to investigate the extent to which heat fluxes in baroclinically unstable flows are consistent with the downgradient flux-gradient relation of Fick's first law and to verify the GEOMETRIC theory of energetic constraints, the eddy flux of temperature or buoyancy is measured from laboratory experiments. We apply multi-level Particle Imaging Velocimetry (Figure 1) (e.g., see Wordsworth (2009)) to measure the velocity field based on the methods of Fincham and Spedding (1997) and Fincham and Delerce (2000) (Sommeria, 2013). From the velocity field, the stream function can be derived using $\psi = \nabla^{-2}\zeta$ via the method of Fiedler (2018). An approximation to the temperature field, $T''(r,\theta,z)$, as a deviation from its horizontal mean, can be obtained using quasi-geostrophic theory from the geostrophic stream function ψ as $T'' = 2\Omega\partial_z\psi/(g\alpha_T)$ (e.g., see Wordsworth (2009)).

Some examples of experimental results of Particle Imaging Velocimetry are illustrated as streamlined snapshots in Figure 2. The reference data are from other past experimental studies (e.g., Hignett et al. (1985) and Mason (1975)). The flow regime diagram is plotted with the reference data and codes adapted from Scolan and Read (2017). The velocity fields are derived by optimizing the correlation between pairs of images of neutrally buoyant tracer particles in time series using the software package UVMAT (Sommeria, 2013), which implements the methods presented by Fincham and Spedding (1997) and Fincham and Delerce (2000); the parameter settings are adapted from the previous work of Scolan and Read (2017). In Figure 2, the flow patterns at faster rotation

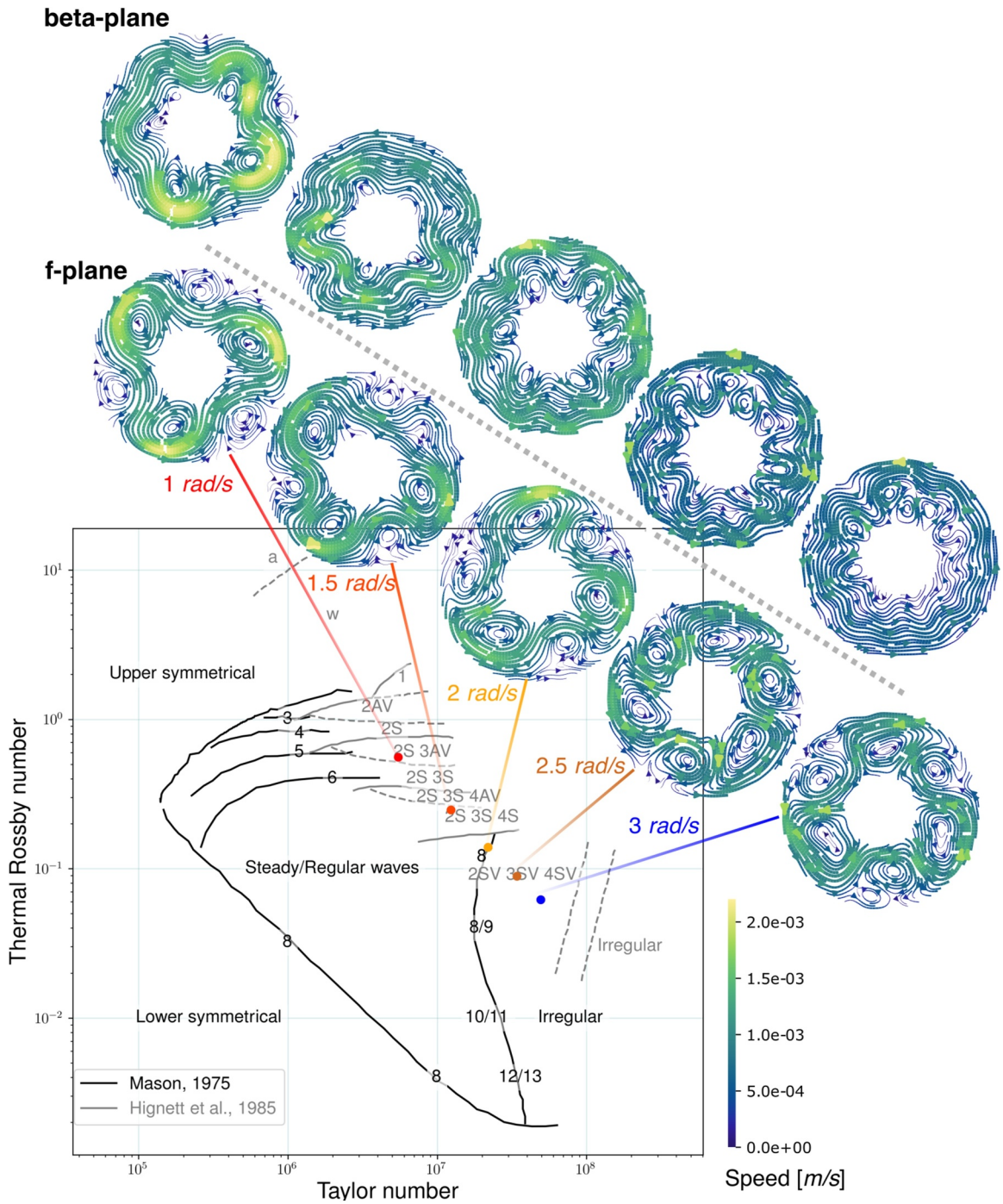

Figure 2. Flow regimes. The flow regime diagram (Hide, 1969; Hide & Mason, 1975) includes the references of past experimental results (Hignett et al., 1985; Mason, 1975). It is plotted with the codes and data adapted from Scolan and Read (2017). The diagram is defined by the Thermal Rossby number $\left(U_T/(f_0 L) = g\alpha_T \Delta T_h H/(\Omega^2 L^2)\right)$ and the Taylor number $\left(4\Omega^2 L^5/(\nu^2 H) \approx \left((\mathbf{f} \times \mathbf{u})/(\nu \nabla^2 \mathbf{u})\right)^2\right)$ (Hide, 1958; Hide & Fowlis, 1965; Wordsworth, 2009). The flow regime S stands for Steady, AV stands for Amplitude Vacillation, and SV stands for Structural Vacillation (Hignett et al., 1985; Mason, 1975).

rates with a beta effect are generally observed to exhibit larger dominant wavenumbers and smaller eddy length scales than the f-plane configuration at similar parameter settings.

The laboratory measurements are supplemented by numerical simulations (Pérez et al., 2010) to estimate values of variables not measured directly—specifically the mean buoyancy frequency, N_0. The simulations are

conducted with the MITgcm (J. Marshall et al., 1997) and adapted from the rotating tank tutorial (Adcroft et al., 2018) with parameter settings consistent with previous experimental and numerical model studies (Hignett et al., 1985; Pérez et al., 2010). The model is configured to be non-hydrostatic, with the vector-invariant formulation of the momentum equations, and with no-slip conditions on all boundaries surrounding the fluid domain. The thermal side boundaries are set with metallic thermal diffusivities of copper for the inner boundary and brass for the outer boundary, consistent with the laboratory experiments. The simulation results have been compared with studies of Read (2003) and Pérez et al. (2010) using the MORALS model (Young & Read, 2008) for f-plane axisymmetric simulations, which show consistent results in terms of the variations of general field structures and heat transport with the Nusselt numbers. More details of the simulations are discussed in the Supporting Information S1.

Although the simulated N_0 varies spatially, and also shows some sensitivity to zonal model resolution, N_0 is found to lie within a relatively narrow range of 0.21–0.28 s^{-1} at the middle height level (7 cm) across all of the experiments included this analysis, all of which have the 4 K temperature contrast. Therefore, the horizontal mean of the buoyancy frequency N_0 is approximated as a constant value, 0.25 s^{-1} at this level, at which the eddy fluxes are measured and analyzed. We note that this estimated value N_0 is broadly consistent with the theoretical estimate $N_0 = \sqrt{g\alpha_T d_z T} \approx \sqrt{g\alpha_T d_r T\, L/H} \sim 0.3\ s^{-1}$, following Hide and Mason (1975).

3. Measured Energetic Constraints

The analysis of the eddy fluxes of temperature and buoyancy are shown in Figure 3, which is to test the applicability of Fick's law to the eddy temperature fluxes, and of the GEOMETRIC energetic constraint to the eddy buoyancy fluxes. Figure 3 shows the analysis based on the experimental PIV measurements of the eddy fluxes of temperature and buoyancy as well as the eddy total energy. The buoyancy frequency is prescribed to be the constant 0.25 s^{-1}, consistent with the numerical simulations (see Section 2, where 4 K temperature contrast is maintained between the side wall thermal boundaries). For further details see Table S1 in Supporting Information S1.

Shown in the first row of Figure 3 are scatter plots of the eddy temperature fluxes against the mean radial temperature gradients. In subplot a, the experimental result is shown in the f-plane case at 1 rad/s: the finding is consistent with the simulations of Pérez et al. (2010), which shows that, while the eddy temperature flux is mostly down-gradient, the relationship between the eddy temperature flux and the mean gradient is complex and non-monotonic. In subplot b, the beta-plane results at 1 rad/s reveal a clearer down-gradient relation between eddy heat fluxes and mean temperature gradients, which broadly supports the use of a Fickian down-gradient closure in this case. However, the beta-plane results do not indicate a simple linear relation between the eddy heat fluxes and mean temperature gradients in all flow regimes. For example, in subplot c at 3 rad/s, there is a clear departure from a monotonic down-gradient relation, which corresponds to data from the inner zone of the annulus channel, where the eddies are separated from the outer zone of the jet pattern (see Figure 2).

The results testing the energetic constraints proposed in the GEOMETRIC framework (D. P. Marshall et al., 2012) are shown in the second row of Figure 3. The inequality between total eddy buoyancy flux and the product of the eddy energy and buoyancy frequency is satisfied in both the f-plane and beta-plane data, which are bounded below the slope ratio of 1 (the shaded region is where the ratio is above 1, which is theoretically impossible). Notably, the relation between the total eddy buoyancy flux and the product of the eddy energy and buoyancy frequency is observed to be approximately linear in the beta-plane cases. Even in the f-plane cases, the relation in the scatter plots is far more monotonic than in the upper panel, and might be approximated as roughly linear.

The equivalent relations between the radial component of the eddy buoyancy flux and the product of the eddy energy and buoyancy frequency are plotted in the third row of Figure 3. The inequality between radial eddy buoyancy flux and the product of the eddy energy and buoyancy frequency is satisfied, for both f-plane and beta-plane cases, as must be the case since $|R| \leq \sqrt{R^2 + S^2}$.

With the observation of an approximately linear relation between the eddy buoyancy fluxes and the product of the eddy energy and buoyancy frequency, the eddy transport efficiency parameter α (Equation 2) can be quantified by linear regression. These values are shown on each panel both the total and radial eddy buoyancy fluxes, and vary

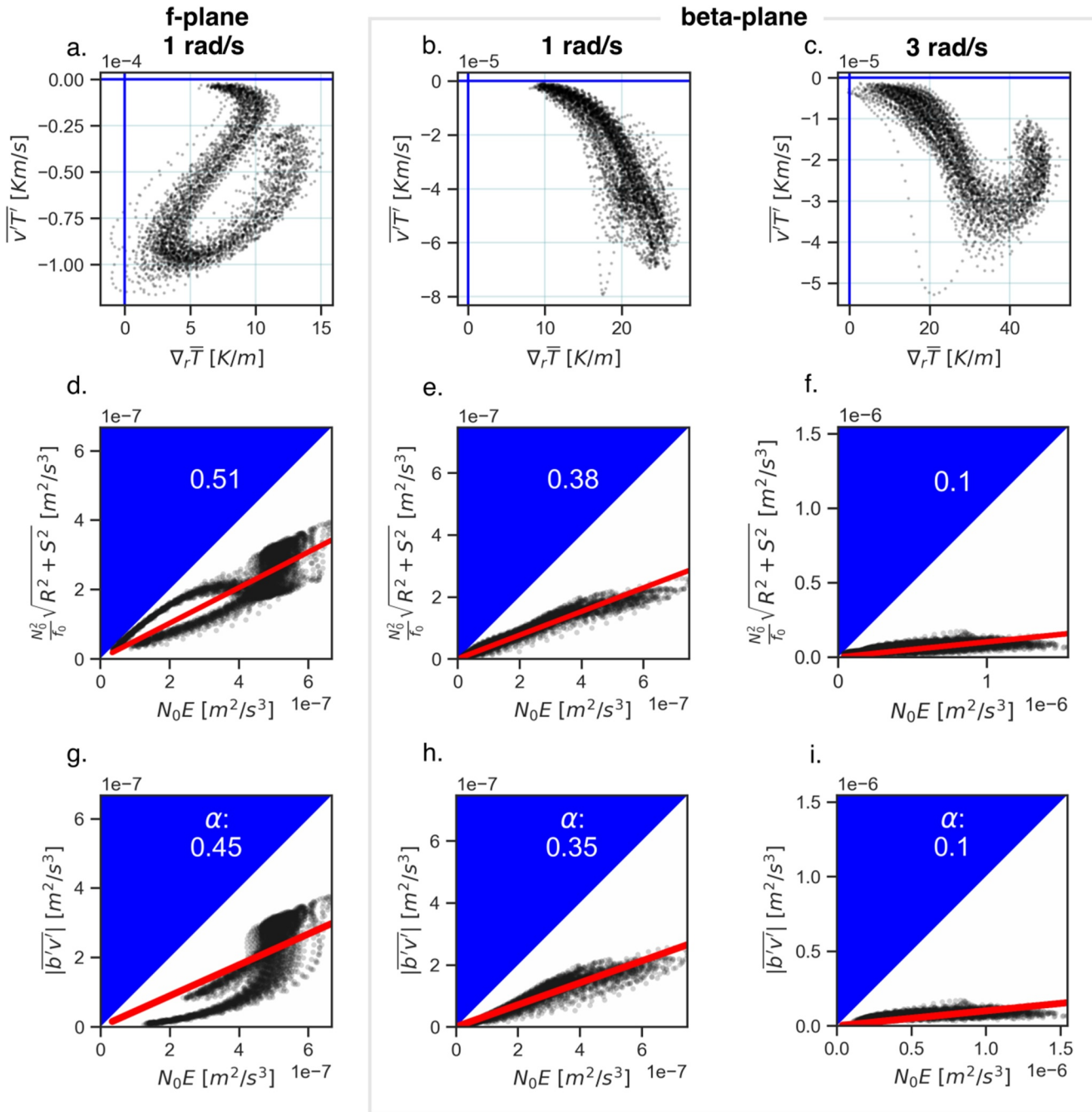

Figure 3. Hypothesis tests. For the Fickian tests on the downgradient relation, the scatter plots show the eddy temperature fluxes versus the radial gradient of zonal mean temperature for the f-plane (a) and the beta-plane (b). At 3 rad/s (c), the beta-plane case still shows features of functional dependency but is not as linear as the 1 rad/s case. For the energetic constraint tests of the GEOMETRIC theory, the second row shows the total buoyancy flux is bounded by the total eddy energy (d, e, and f). The third row shows the ratio of radial buoyancy flux versus total eddy energy is approximately linear for the beta-plane cases (h and i, instead of g). These cases are for the 4 K temperature contrast, the rotation rate of 1 rad/s, and the middle height level at 7 cm. The data dots are the pointwise experimental values of velocity and estimated temperature at different values of r and θ at the height level indicated, calculated from PIV velocity measurements along with an estimate of the buoyancy frequency from corresponding numerical simulations for each full round of PIV data collection.

between 0.5 at low rotation rates/on the f-plane and 0.1 at higher rotation rates on the beta-plane. These values are broadly consistent, to within experimental uncertainty, with those obtained for the linear Eady theory (≃0.6; D. P. Marshall et al. (2012)) and in fully nonlinear simulations of the Eady instability problem (≃0.2; based on Bachman et al. (2017)). Moreover, Figure 2a of Bachman et al. (2017) reveals a decline in the value of the eddy

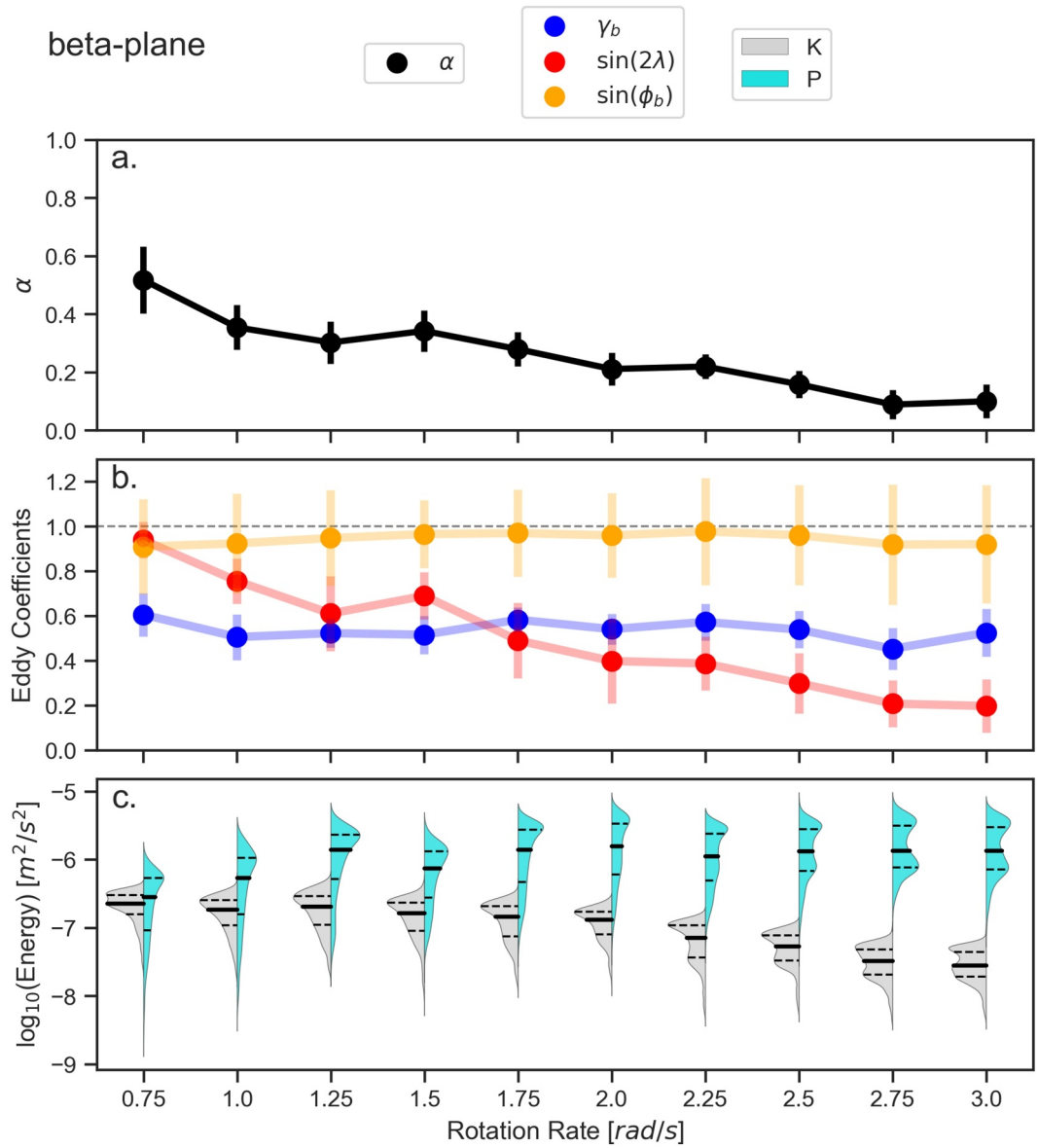

Figure 4. Eddy transport efficiency with a beta effect. (a) The eddy coefficient α with faster rotation rates shows a generally declining trend. (b) The decomposition of α by the GEOMETRIC definition shows the energy partition term ($\sin 2\lambda$) as the main decreasing factor. (c) The decreasing energy partition is associated with the generally increasing difference in total eddy energy (E) between the eddy kinetic energy (K) and eddy available potential energy (P) for the increasing rotation rates. Here the error bars are estimated from the standard deviation of the ratio data.

transport efficiency parameter α as the flow becomes more nonlinear (i.e., higher eddy diffusivity), indicated by the slight mismatch between the slope of the measured line and theoretical prediction in that figure. Likewise, in the laboratory experiments, a decline is observed in α at the higher rotation rate, where the flow is more nonlinear (Figure 2).

Figure 4 shows the analysis of the efficiency of eddy heat transport following the GEOMETRIC theory. For the experimental results shown in Figure 4, the causes of the decline in eddy transport efficiency parameter α with the rotation rate is investigated further for the beta-plane cases with the radial temperature contrast held constant. The eddy transport efficiency measured by the non-dimensional coefficient α in Equation 2 shows a general decreasing trend with the faster rotations (subplot a). This general decline in eddy transport efficiency is dominated by the general decreasing trend in the energy partition term $\left(\sin(2\lambda) = 2\sqrt{KP/E^2}\right)$ (subplot b). The

decreasing eddy transport efficiency is dominated by declining energy partition in the total eddy energy between eddy kinetic energy and eddy available potential energy components (subplot c). We note that these conclusions are unaffected by the subtle variations found in N_0 across the numerical simulations (not shown).

The decrease in the energy partition and eddy transport efficiency as the rotation rate is increased can be interpreted through the associated decrease in the Burger number, $g\alpha_T \Delta T_w H/\left(4\Omega^2 L^2\right)$. The Burger number is in turn related to the Thermal Rossby number, $g\alpha_T \Delta T_h H/(\Omega^2 L^2$, for an annulus with the same temperature difference in the vertical and horizontal directions. The values of the Thermal Rossby Number are indicated in Figure 2, with higher values corresponding to the more nonlinear flow regimes, where α is expected to be lower.

Finally, we note that in the empirical model proposed by Wei et al. (2024) for eddy fluxes in the presence of a topographic slope, the eddy efficiency α is expected to increase as the rotation rate is increased, in contrast to the findings reported above. Nevertheless, Wei et al. (2022) also suggest that the topographic slope might reduce the efficiency of the eddy buoyancy fluxes in beta-plane experiments. We note that the eddy efficiency is indeed lower with a topographic beta plane compared with the f-plane, consistent with this argument.

In summary, the above results provide direct experimental measurements in support of the energetically constrained and down-gradient eddy buoyancy fluxes as hypothesized in the GEOMETRIC framework (D. P. Marshall et al., 2012). Moreover, these results are consistent with the previous numerical calculations of Bachman et al. (2017), despite a fundamental difference in the nature of the boundary conditions between the two studies. In the present laboratory experiments, the rigid upper and lower boundaries impose both upper and lower no-slip conditions. In contrast, in the numerical calculations of Bachman et al. (2017), and the ocean, the upper boundary is a free surface that allows water to slip freely (aside from the relative stress due to the difference between oceanic and atmospheric velocities). The effect of imposing a no-slip condition at the sea surface is seen in the numerical calculations of Meneghello et al. (2021) with the growth and decay of mesoscale eddies as sea ice recedes and grows. However, the assumptions of the GEOMETRIC framework do not rely on the presence or otherwise of a free-slip surface boundary. The more complicated functional relations between the eddy fluxes and mean temperature gradient or eddy energy observed with the f-plane cases in Figure 3 may suggest roles for additional variables beyond those considered here. However, the investigation of these dependencies is beyond the scope of this study.

4. Conclusions

Baroclinic eddy heat and buoyancy fluxes transport have been measured in rotating annulus laboratory experiments to test the hypotheses employed in eddy parameterization theories. We have evaluated the impact of a topographic beta effect on the energetic constraints on eddy buoyancy flux and the generalized Fickian assumption of temperature down-gradient diffusion. With a beta effect, approximate linearity is observed between the eddy buoyancy fluxes and total eddy energy. The efficiency of eddy transport is quantified by the nondimensional eddy transport coefficient in different measured flow regimes. In the flow regimes with the lower Thermal Rossby numbers, this coefficient generally decreases, associated with the change of energy partition between eddy available potential energy and eddy kinetic energy and the transition to a more nonlinear flow regime. A more complicated dependence of heat transport on experimental parameters is observed in the f-plane data, consistent with the numerical simulations of Pérez et al. (2010), and seems to suggest extra variable dependencies that are as yet unclear.

Several factors in the experiments limit the accuracy and precision of the measurements, such as in the control of the switching time between different light levels which contributed to uncertainties in temperature estimation from PIV measurements, although exploratory tests suggest that the main conclusions of this paper are not qualitatively affected by these limitations. Nevertheless, this should be a topic for further investigation, and future studies could explore other light control designs (Ravela et al., 2010) to reduce the time delay in multi-height samplings for better measurements of eddy transport efficiencies.

Further limitations with the data processing arise from making the quasi-geostrophic assumption, applied to estimate the horizontal deviation of temperatures, although analysis of the numerical simulations suggests the main conclusions are qualitatively unaffected. The discrete sampling of the velocity field at a small number of vertical levels could be better optimized in future experiments by exploiting the data from numerical simulations. The present study is also limited to wave-dominated flow regimes due to the size and accessible rotation rates of

the experimental apparatus. Future studies should investigate flows in more nonlinear regimes, including further investigation of the general applicability for multi-scale flows (Taylor & Thompson, 2023), the atmosphere (Schemm & Rivière, 2019), ocean (Mak et al., 2018), and planetary systems (Battalio et al., 2016).

In summary, the laboratory results with a topographic beta effect broadly support Fick's first law, and provide the first direct experimental evidence in support of the GEOMETRIC framework in which eddy buoyancy flux is constrained by total eddy energy. With the topographic beta effect, a relatively simple relation is observed between the eddy buoyancy flux and the total eddy energy, with the ratio quantifying the eddy transport efficiency. This efficiency decreases in more complex flow regimes with larger rotation rates, associated with the changing energy partition between eddy available potential energy and eddy kinetic energy.

Finally, we hope that this study has demonstrated the potential for controlled laboratory experiments to provide valuable insights into the nature of eddy fluxes in rotating, stratified flows. An interesting topic for further investigation using a rotating annulus might be the impact of a topographic barrier on the eddy fluxes. For example, it is known that eddy buoyancy fluxes are enhanced greatly downstream of topographic features (MacCready & Rhines, 2001), and likewise eddy Reynolds stresses (Tansley & Marshall, 2001). In contrast, the numerical results in D. P. Marshall et al. (2017) suggest the limited impact on the zonally-integrated eddy buoyancy fluxes, despite these marked zonal variations. Nevertheless, many details remain poorly understood.

Data Availability Statement

PIV data samples (Qian et al., 2024b) are described in Supporting Information S1, where UVMAT (Sommeria, 2013) with the methods of Fincham and Spedding (1997) and Fincham and Delerce (2000) has been applied. Further processing is built on the work of Wordsworth et al. (2008), Scolan and Read (2017), Wright et al. (2017), and Fiedler (2018). The MITgcm (J. Marshall et al., 1997; Adcroft et al., 2018) has been applied in the simulation with version checkpoint67c. Related samples and codes (Qian et al., 2024a, 2024b) are discussed in Supporting Information S1. The MORALS model (Pérez et al., 2010; Young, 2015; Young & Read, 2008) has also been applied with version 150506.

Acknowledgments
We would like to thank Andy Clack, Hélène Scolan, Bob Watkins and others for the help and advice. P. L. R. would like to thank UKRI for research funding (Grants ST/S000461/1 and EP/W022087/1). We are grateful to two anonymous reviewers whose detailed comments greatly improved the final manuscript.

References

Adcroft, A., Campin, J.-M., Dutkiewicz, S., Evangelinos, C., Ferreira, D., Forget, G., et al. (2018). MITgcm user manual. Retrieved from https://dspace.mit.edu/handle/1721.1/117188, https://mitgcm.readthedocs.io/en/latest/

Bachman, S., Marshall, D., Maddison, J., & Mak, J. (2017). Evaluation of a scalar eddy transport coefficient based on geometric constraints. *Ocean Modelling*, *109*, 44–54. https://doi.org/10.1016/j.ocemod.2016.12.004

Bastin, M. E., & Read, P. L. (1997). A laboratory study of baroclinic waves and turbulence in an internally heated rotating fluid annulus with sloping endwalls. *Journal of Fluid Mechanics*, *339*, 173–198. https://doi.org/10.1017/S0022112097005259

Battalio, M., Szunyogh, I., & Lemmon, M. (2016). Energetics of the martian atmosphere using the Mars analysis correction data assimilation (MACDA) dataset. *Icarus*, *276*, 1–20. https://doi.org/10.1016/j.icarus.2016.04.028

Eady, E. T. (1949). Long waves and cyclone waves. *Tellus*, *1*(3), 33–52. https://doi.org/10.1111/j.2153-3490.1949.tb01265.x

Eden, C., & Greatbatch, R. J. (2008). Towards a mesoscale eddy closure. *Ocean Modelling*, *20*(3), 223–239. https://doi.org/10.1016/j.ocemod.2007.09.002

Fiedler, B. (2018). Two-dimensional flows: Vorticity and stream function method. https://github.com/bfiedler/metr4323/blob/main/N090_streamfunctionvorticity2d.ipynb

Fincham, A., & Delerce, G. (2000). Advanced optimization of correlation imaging velocimetry algorithms. *Experiments in Fluids*, *29*(7), S013–S022. https://doi.org/10.1007/s003480070003

Fincham, A., & Spedding, G. (1997). Low cost, high resolution DPIV for measurement of turbulent fluid flow. *Experiments in Fluids*, *23*(6), 449–462. https://doi.org/10.1007/s003480050135

Fultz, D., & Kaylor, R. (1959). The propagation of frequency in experimental baroclinic waves in a rotating annular ring. In B. Bolin (Ed), *The Atmosphere and the sea in motion* (pp. 359–371). The Rockefeller Institute Press.

Gent, P. R., & McWilliams, J. C. (1990). Isopycnal mixing in ocean circulation models. *Journal of Physical Oceanography*, *20*(1), 150–155. https://doi.org/10.1175/1520-0485(1990)020⟨0150:IMIOCM⟩2.0.CO;2

Gent, P. R., Willebrand, J., McDougall, T. J., & McWilliams, J. C. (1995). Parameterizing eddy-induced tracer transports in ocean circulation models. *Journal of Physical Oceanography*, *25*(4), 463–474. https://doi.org/10.1175/1520-0485(1995)025⟨0463:PEITTI⟩2.0.CO;2

Green, J. S. A. (1970). Transfer properties of the large-scale eddies and the general circulation of the atmosphere. *Quarterly Journal of the Royal Meteorological Society*, *96*(408), 157–185. https://doi.org/10.1002/qj.49709640802

Hide, R. (1953). Some experiments on thermal convection in a rotating liquid. *Quarterly Journal of the Royal Meteorological Society*, *79*(339), 161. https://doi.org/10.1002/qj.49707933916

Hide, R. (1958). An experimental study of thermal convection in a rotating liquid. *Philosophical Transactions of the Royal Society of London - Series A: Mathematical and Physical Sciences*, *250*(983), 441–478. https://doi.org/10.1098/rsta.1958.0004

Hide, R. (1969). Some laboratory experiments on free thermal convection in a rotating fluid subject to a horizontal temperature gradient and their relation to the theory of the global atmospheric circulation. In G. A. Corby (Ed.), *The global circulation of the atmosphere*. Royal Meteorological Society.

Hide, R. (1977). Experiments with rotating fluids. *Quarterly Journal of the Royal Meteorological Society*, *103*(435), 1–28. https://doi.org/10.1002/qj.49710343502

Hide, R., & Fowlis, W. W. (1965). Thermal convection in a rotating annulus of liquid: Effect of viscosity on the transition between axisymmetric and non-axisymmetric flow regimes. *Journal of the Atmospheric Sciences*, *22*(5), 541–558. https://doi.org/10.1175/1520-0469(1965)022⟨0541:TCIARA⟩2.0.CO;2

Hide, R., & Mason, P. J. (1975). Sloping convection in a rotating fluid. *Advances in Physics*, *24*(1), 47–100. https://doi.org/10.1080/00018737500101371

Hignett, P., White, A. A., Carter, R. D., Jackson, W. D. N., & Small, R. M. (1985). A comparison of laboratory measurements and numerical simulations of baroclinic wave flows in a rotating cylindrical annulus. *Quarterly Journal of the Royal Meteorological Society*, *111*(467), 131–154. https://doi.org/10.1002/qj.49711146705

Isachsen, P. E. (2011). Baroclinic instability and eddy tracer transport across sloping bottom topography: How well does a modified eady model do in primitive equation simulations? *Ocean Modelling*, *39*(1), 183–199. https://doi.org/10.1016/j.ocemod.2010.09.007

Leovy, C. B. (1969). Mars: Theoretical aspects of meteorology. *Applied Optics*, *8*(7), 1279–1286. https://doi.org/10.1364/AO.8.001279

Lorenz, E. N. (1955). Available potential energy and the maintenance of the general circulation. *Tellus*, *7*(2), 157–167. https://doi.org/10.1111/j.2153-3490.1955.tb01148.x

Lorenz, E. N. (1967). *The nature and theory of the general circulation of the atmosphere*. World Meteorological Organization.

MacCready, P., & Rhines, P. B. (2001). Meridional transport across a zonal channel: Topographic localization. *Journal of Physical Oceanography*, *31*(6), 1427–1439. https://doi.org/10.1175/1520-0485(2001)031⟨1427:MTAAZC⟩2.0.CO;2

Mak, J., Maddison, J. R., Marshall, D. P., & Munday, D. R. (2018). Implementation of a geometrically informed and energetically constrained mesoscale eddy parameterization in an ocean circulation model. *Journal of Physical Oceanography*, *48*(10), 2363–2382. https://doi.org/10.1175/JPO-D-18-0017.1

Mak, J., Marshall, D., Maddison, J., & Bachman, S. (2017). Emergent eddy saturation from an energy constrained eddy parameterisation. *Ocean Modelling*, *112*, 125–138. https://doi.org/10.1016/j.ocemod.2017.02.007

Mak, J., Marshall, D. P., Madec, G., & Maddison, J. R. (2022). Acute sensitivity of global ocean circulation and heat content to eddy energy dissipation timescale. *Geophysical Research Letters*, *49*(8), e2021GL097259. https://doi.org/10.1029/2021GL097259

Marshall, D. P., & Adcroft, A. J. (2010). Parameterization of ocean eddies: Potential vorticity mixing, energetics and Arnold's first stability theorem. *Ocean Modelling*, *32*(3), 188–204. (The magic of modelling: A special volume commemorating the contributions of Peter D. Killworth – Part 2). https://doi.org/10.1016/j.ocemod.2010.02.001

Marshall, D. P., Ambaum, M. H. P., Maddison, J. R., Munday, D. R., & Novak, L. (2017). Eddy saturation and frictional control of the Antarctic Circumpolar Current. *Geophysical Research Letters*, *44*(1), 286–292. https://doi.org/10.1002/2016GL071702

Marshall, D. P., Maddison, J. R., & Berloff, P. S. (2012). A framework for parameterizing eddy potential vorticity fluxes. *Journal of Physical Oceanography*, *42*(4), 539–557. https://doi.org/10.1175/JPO-D-11-048.1

Marshall, J., Adcroft, A., Hill, C., Perelman, L., & Heisey, C. (1997). A finite-volume, incompressible Navier Stokes model for studies of the ocean on parallel computers. *Journal of Geophysical Research*, *102*(C3), 5753–5766. https://doi.org/10.1029/96JC02775

Marshall, J., & Plumb, R. A. (2007). *Atmosphere, ocean and climate dynamics: An introductory text*. Academic Press.

Mason, P. J. (1975). Baroclinic waves in a container with sloping end walls. *Philosophical Transactions of the Royal Society of London A: Mathematical, Physical and Engineering Sciences*, *278*(1284), 397–445. https://doi.org/10.1098/rsta.1975.0032

Meneghello, G., Marshall, J., Lique, C., Isachsen, P. E., Doddridge, E., Campin, J.-M., et al. (2021). Genesis and decay of mesoscale baroclinic eddies in the seasonally ice-covered interior arctic ocean. *Journal of Physical Oceanography*, *51*(1), 115–129. https://doi.org/10.1175/JPO-D-20-0054.1

Pérez, E. P., Read, P. L., & Moroz, I. M. (2010). Assessing eddy parameterization schemes in a differentially heated rotating annulus experiment. *Ocean Modelling*, *32*(3), 118–131. https://doi.org/10.1016/j.ocemod.2009.11.003

Pfeffer, R. L., & Barcilon, A. (1978). Determination of eddy fluxes of heat and eddy temperature variances using weakly nonlinear theory. *Journal of the Atmospheric Sciences*, *35*(11), 2099–2110. https://doi.org/10.1175/1520-0469(1978)035⟨2099:DOEFOH⟩2.0.CO;2

Qian, C., Read, P., & Marshall, D. P. (2024a). Codes for "Energetic constraints on baroclinic eddy heat transport with a beta effect in the laboratory" [Software]. *GitHub*. https://github.com/cctsien/EnergeticConstraints

Qian, C., Read, P., & Marshall, D. P. (2024b). Data for "Energetic constraints on baroclinic eddy heat transport with a beta effect in the laboratory [Dataset]. *Oxford University Research Archive*. https://ora.ox.ac.uk/objects/uuid:99890c63-7f57-4ebe-83cf-4d0e7247d345

Ravela, S., Marshall, J., Hill, C., Wong, A., & Stransky, S. (2010). A realtime observatory for laboratory simulation of planetary flows. *Experiments in Fluids*, *48*(5), 915–925. https://doi.org/10.1007/s00348-009-0752-0

Read, P. L. (2003). A combined laboratory and numerical study of heat transport by baroclinic eddies and axisymmetric flows. *Journal of Fluid Mechanics*, *489*, 301–323. https://doi.org/10.1017/S002211200300524X

Read, P. L., Pérez, E. P., Moroz, I. M., & Young, R. M. B. (2014). General circulation of planetary atmospheres. In (Eds), T. von Larcher, & P. D. Williams, *Modeling atmospheric and oceanic flows: Insights from laboratory experiments and numerical simulations* (pp. 7–44). American Geophysical Union. https://doi.org/10.1002/9781118856024.ch1

Schemm, S., & Rivière, G. (2019). On the efficiency of baroclinic eddy growth and how it reduces the north pacific storm-track intensity in midwinter. *Journal of Climate*, *32*(23), 8373–8398. https://doi.org/10.1175/JCLI-D-19-0115.1

Scolan, H., & Read, P. L. (2017). A rotating annulus driven by localized convective forcing: A new atmosphere-like experiment. *Experiments in Fluids*, *58*(6), 75. https://doi.org/10.1007/s00348-017-2347-5

Sommeria, J. (2013). UVMAT. Retrieved from http://servforge.legi.grenoble-inp.fr/projects/soft-uvmat

Stone, P. (1972). A simplified radiative-dynamical model for the static stability of rotating atmospheres. *Journal of the Atmospheric Sciences*, *29*(3), 405–418. https://doi.org/10.1175/1520-0469(1972)029⟨0405:ASRDMF⟩2.0.CO;2

Tansley, C. E., & Marshall, D. P. (2001). Flow past a cylinder on a β plane, with application to Gulf Stream separation and the Antarctic Circumpolar Current. *Journal of Physical Oceanography*, *31*(11), 3274–3283. https://doi.org/10.1175/1520-0485(2001)031⟨3274:FPACOA⟩2.0.CO;2

Taylor, J. R., & Thompson, A. F. (2023). Submesoscale dynamics in the upper ocean. *Annual Review of Fluid Mechanics*, *55*(1), 103–127. https://doi.org/10.1146/annurev-fluid-031422-095147

Vallis, G. K. (2017). *Atmospheric and oceanic fluid dynamics: Fundamentals and large-scale circulation* (2nd ed.). Cambridge University Press. https://doi.org/10.1017/9781107588417

Vincze, M., Harlander, U., von Larcher, T., & Egbers, C. (2014). An experimental study of regime transitions in a differentially heated baroclinic annulus with flat and sloping bottom topographies. *Nonlinear Processes in Geophysics*, *21*(1), 237–250. https://doi.org/10.5194/npg-21-237-2014

Visbeck, M., Marshall, J., Haine, T., & Spall, M. (1997). Specification of eddy transfer coefficients in coarse-resolution ocean circulation models. *Journal of Physical Oceanography*, *27*(3), 381–402. https://doi.org/10.1175/1520-0485(1997)027⟨0381:SOETCI⟩2.0.CO;2

von Larcher, T., Fournier, A., & Hollerbach, R. (2013). The influence of a sloping bottom endwall on the linear stability in the thermally driven baroclinic annulus with a free surface. *Theoretical and Computational Fluid Dynamics*, *27*(3–4), 433–451. https://doi.org/10.1007/s00162-012-0289-3

Wei, H., Wang, Y., & Mak, J. (2024). Parameterizing eddy buoyancy fluxes across prograde shelf/slope fronts using a slope-aware GEOMETRIC closure. *Journal of Physical Oceanography*, *54*(2), 359–377. https://doi.org/10.1175/JPO-D-23-0152.1

Wei, H., Wang, Y., Stewart, A. L., & Mak, J. (2022). Scalings for eddy buoyancy fluxes across prograde shelf/slope fronts. *Journal of Advances in Modeling Earth Systems*, *14*(12), e2022MS003229. https://doi.org/10.1029/2022MS003229

Wordsworth, R. D. (2009). *Theoretical and experimental investigations of turbulent jet formation in planetary fluid dynamics*. University of Oxford.

Wordsworth, R. D., Read, P. L., & Yamazaki, Y. H. (2008). Turbulence, waves, and jets in a differentially heated rotating annulus experiment. *Physics of Fluids*, *20*(12), 126602. https://doi.org/10.1063/1.2990042

Wright, S., Su, S., Scolan, H., Young, R. M. B., & Read, P. L. (2017). Regimes of axisymmetric flow and scaling laws in a rotating annulus with local convective forcing. *Fluids*, *2*(3), 41. https://doi.org/10.3390/fluids2030041

Young, R. M. B. (2015). Met. Office/Oxford rotating annulus laboratory simulation (MORALS). Retrieved from https://www2.physics.ox.ac.uk/research/geophysical-fluid-dynamics/morals.

Young, R. M. B., & Read, P. L. (2008). Flow transitions resembling bifurcations of the logistic map in simulations of the baroclinic rotating annulus. *Physica D: Nonlinear Phenomena*, *237*(18), 2251–2262. https://doi.org/10.1016/j.physd.2008.02.014